nature neuroscience

Regulation of acetylcholine receptor clustering by ADF/cofilin-directed vesicular trafficking

Chi Wai Lee[1,2], Jianzhong Han[2], James R Bamburg[3], Liang Han[1,2], Rachel Lynn[1] & James Q Zheng[1,2]

Postsynaptic receptor localization is crucial for synapse development and function, but the underlying cytoskeletal mechanisms remain elusive. Using *Xenopus* neuromuscular junctions as a model, we found that actin depolymerizing factor (ADF)/cofilin regulated actin-dependent vesicular trafficking of acetylcholine receptors (AChRs) to the postsynaptic membrane. Active ADF/cofilin was concentrated in small puncta adjacent to AChR clusters and was spatiotemporally correlated with the formation and maintenance of surface AChR clusters. Notably, increased actin dynamics, vesicular markers and intracellular AChRs were all enriched at the sites of ADF/cofilin localization. Furthermore, a substantial amount of new AChRs was detected at these ADF/cofilin-enriched sites. Manipulation of either ADF/cofilin activity through its serine-3 phosphorylation or ADF/cofilin localization via 14-3-3 proteins markedly attenuated AChR insertion and clustering. These results suggest that spatiotemporally restricted ADF/cofilin-mediated actin dynamics regulate AChR trafficking during the development of neuromuscular synapses.

Chemical synapses represent a major form of neuronal connections in the vertebrate nervous system that underlie a wide spectrum of neural functions. A prominent feature of chemical synapses is the presence of a postsynaptic apparatus containing highly concentrated receptors for effective reception of neurotransmitters released from the presynaptic nerve terminal. Regulation of postsynaptic receptor localization is therefore crucial for synapse formation, function and modulation[1–3]. At present, the cellular mechanisms underlying the spatiotemporal control of receptor trafficking and clustering at the postsynaptic site remain poorly understood. Because of its size, accessibility and simplicity[4], the neuromuscular junction (NMJ) is a good model for studying the spatial distribution and trafficking of postsynaptic AChRs. Previous studies have shown that aneural AChR clusters can spontaneously form in the absence of innervation and nerve-secreted factors *in vivo*[5]. Nerve innervation, however, induces site-directed clustering of AChRs through redistribution from aneural clusters, recruitment of diffuse receptors and new synthesis from the subsynaptic nuclei[4,6]. Two counteracting nerve-derived factors, agrin and acetylcholine, regulate the redistribution of AChRs on the muscle membrane[7]. Agrin activates muscle-specific tyrosine kinase (MuSK) for inducing AChR clustering on the postsynaptic membrane[8], whereas acetylcholine disperses extrasynaptic AChR clusters[9,10].

It remains unclear how AChRs are spatiotemporally delivered to the synaptic site during synapse formation. Passive diffusion trap and/or active trafficking mechanisms may be involved in AChR redistribution[11,12]. Clustered AChRs are believed to be immobilized via scaffolding connections to the actin cytoskeleton[13,14], thus their redistribution probably requires dynamic changes in the cortical actin network. We used a combination of live-cell imaging and molecular and pharmacological manipulations to investigate the cytoskeletal control of AChR trafficking during synapse formation. We found that ADF/cofilin is important for synaptic targeting of AChRs. ADF/cofilin accumulated at the nascent synaptic site before the clustering of surface AChRs. Furthermore, the disassembly of the spontaneous AChR clusters was preceded by the disappearance of active ADF/cofilin aggregates. Localized ADF/cofilin was associated with increased dynamic actin turnover and spatially correlated with the surface delivery of intracellular AChRs through vesicular trafficking. We identified that 14-3-3 molecules are essential for the spatial localization of ADF/cofilin for the regulation of AChR trafficking. Finally, alteration of ADF/cofilin activity or disruption of its localization prevented the formation of new AChR clusters induced by synaptogenic stimuli. These findings indicate that spatiotemporally restricted ADF/cofilin-controlled actin dynamics regulate the surface targeting of postsynaptic receptors at synaptic sites.

RESULTS

Active ADF/cofilin localizes at AChR clusters

Nerve-independent AChR clusters can spontaneously develop on muscle surface in culture on matrix-coated substrate and have an elaborately perforated pattern with a marked similarity to synaptic AChR clusters at the NMJs *in vivo*[4,15]. Similarly, spontaneous AChR clusters were observed in embryonic *Xenopus* muscle cells cultured on laminin-containing attachment matrix[16], as visualized by live labeling with rhodamine-conjugated α-bungarotoxin (Rh-BTX; **Fig. 1a**). To examine the role of ADF/cofilin in AChR clustering, we labeled AChRs in live cells with Rh-BTX and then fixed and immunostained either the total *Xenopus* ADF/cofilin (XAC) or the inactive phosphoserine-3 XAC

[1]Department of Cell Biology, Emory University School of Medicine, Atlanta, Georgia, USA. [2]Department of Neuroscience and Cell Biology, University of Medicine and Dentistry of New Jersey, Robert Wood Johnson Medical School, Piscataway, New Jersey, USA. [3]Department of Biochemistry and Molecular Biology, and Molecular, Cellular and Integrative Neuroscience Program, Colorado State University, Fort Collins, Colorado, USA. Correspondence should be addressed to J.Q.Z. (james.zheng@emory.edu).

Received 6 January; accepted 23 March; published online 31 May 2009; doi:10.1038/nn.2322

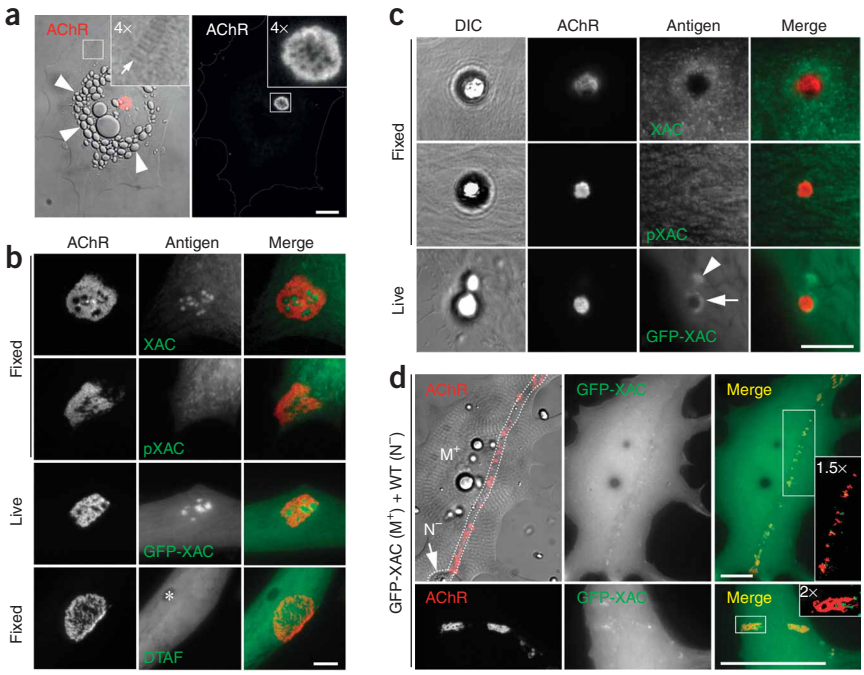

Figure 1 Localization of ADF/cofilin in spontaneous and synaptic AChR clusters. (**a**) Representative differential interference contrast (DIC) and fluorescent images of a 1-d-old cultured *Xenopus* muscle cell showing spontaneous AChR clusters after Rh-BTX labeling. Insets, magnified regions. Arrows indicate striation and arrowheads indicate yolk granules. (**b**) The spatial pattern of spontaneous AChR clusters and XAC in *Xenopus* muscle cells after 5 d in culture. The first and second rows show the distribution of AChRs (Rh-BTX labeling) and endogenous XAC and pXAC (immunostaining). The third row shows the distribution of AChRs and GFP-XAC in a live muscle cell. The bottom row shows the AChR distribution and the cell volume labeled by DTAF. The asterisk indicates a site of volume reduction caused by a yolk granule. (**c**) Agrin bead–induced AChR clustering and XAC localization as revealed by immunostaining in fixed cells or live imaging. The arrow indicates GFP-XAC accumulation around the AChR clusters induced by an agrin bead and the arrowhead indicates GFP-XAC accumulation at an agrin bead contact even without AChRs. (**d**) The spatial distributions of AChR clusters and GFP-XAC at developing neuromuscular junctions in culture. GFP-XAC–expressing muscle cells (M^+) were cocultured with wild-type spinal neurons (N^-) for 3 d. The nerve-muscle contacts are outlined by the dotted lines in the DIC image, which is overlaid with Rh-BTX–labeled AChR signals (red). Another example of AChR clusters and GFP-XAC signals from a different cell are shown in the bottom row. Insets, the boxed region was magnified and pseudo-colored after an intensity threshold. WT, wild type. Scale bars represent 40 μm (**a**,**d**) and 10 μm (**b**,**c**).

(pXAC)[17]. The specificity of these antibodies was verified by our previous studies[18,19], and XAC expression in *Xenopus* muscle tissues was confirmed by RT-PCR and western blotting (**Supplementary Fig. 1** online). We found that XAC was preferentially concentrated as small puncta at the AChR-poor perforations in the spontaneous AChR clusters, whereas pXAC had a uniform distribution (**Fig. 1b**). This complementary pattern of XAC and AChR distributions was also observed by live imaging of muscle cells expressing green fluorescent protein (GFP)-XAC in conjunction with AChR labeling (**Fig. 1b**). Moreover, the localization of GFP-XAC to the AChR-poor perforations was further enhanced by the constitutively active mutation (3A; serine-3 replaced by alanine) but markedly reduced by the inactive mutation (3E; serine-3 replaced by glutamate) (**Supplementary Fig. 2** online). It should be noted that the observed XAC puncta are unlikely to be a result of membrane infoldings, as is seen in mature NMJs, because staining with the volume dye dichlorotriazinylaminofluorescein (DTAF)[20] showed no apparent spatial patterns associated with the spontaneous AChR clusters (**Fig. 1b**). The DTAF fluorescence intensity, however, was reduced at the location of a yolk granule inside the cell, indicating its effectiveness in highlighting the cell volume. Furthermore, confocal imaging revealed that GFP-XAC was localized as puncta underneath the plasma membrane without obvious membrane infoldings (**Supplementary Fig. 3** online). Together, these results indicate that putatively active, nonphosphorylated XAC is preferentially enriched in AChR-poor perforations in these complex structures of spontaneous AChR clusters.

We next tested whether XAC accumulates at the site of AChR clustering during synapse formation. We found that beads coated with an active recombinant agrin C-terminal fragment[21] potently induced AChR clustering (**Fig. 1c**), whereas control BSA-coated or full-length agrin-coated beads were ineffective[22] (**Supplementary Fig. 4** online). Immunostaining showed that XAC accumulated at the agrin bead–muscle contact in a ring pattern surrounding the AChR clusters, whereas pXAC was distributed uniformly (**Fig. 1c**). A similar pattern of XAC and AChR localization was also observed by live imaging of GFP-XAC and AChR (**Fig. 1c** and **Supplementary Fig. 3**). Occasionally, GFP-XAC puncta could be detected at the bead-muscle contact where no AChR clusters had yet been formed (**Fig. 1c**), suggesting a potential temporal difference in the localization of XAC and AChRs induced by agrin beads. We also examined the localization of XAC at neuromuscular synapses in *Xenopus* nerve-muscle cocultures. Live imaging showed that GFP-XAC puncta were distributed closely with AChR clusters along the nerve-contacted trail on the muscle cell (**Fig. 1d**). At higher magnifications, XAC puncta and AChR clusters were localized in a juxtaposing, non-overlapping pattern. In some cases, XAC was also enriched at the AChR-poor perforations in the nerve-induced AChR clusters, showing a similar complementary topography to that of spontaneous AChR clusters. Together, these results show that active, nonphosphorylated XAC localizes to AChR clusters in the spontaneous or synaptic specializations.

Spontaneous AChR clusters undergo slow redistribution in culture (**Supplementary Fig. 5** online), allowing the examination of a spatiotemporal correlation between ADF/cofilin localization and AChR redistribution. In a time-lapse recording, we found that GFP-XAC first concentrated in the perforations of a spontaneous AChR cluster (**Fig. 2a**). Over the course of 40 h of recording, this AChR cluster redistributed to a new location. Apparently, GFP-XAC puncta were detected at the new location at 10 h, whereas detectable AChR clusters were not observed until after 20 h. Notably, the disappearance of localized GFP-XAC at the original AChR cluster was found to precede the gradual disassembly of the AChR clusters. This spatiotemporal relationship was better demonstrated after AChR clusters and GFP-XAC puncta were highlighted with red and green pseudo-colors, respectively.

At developing NMJs, nerve-induced AChR clustering on the postsynaptic membrane is accompanied by the dispersal of the spontaneous AChR clusters[23]. We therefore performed similar time-lapse recordings

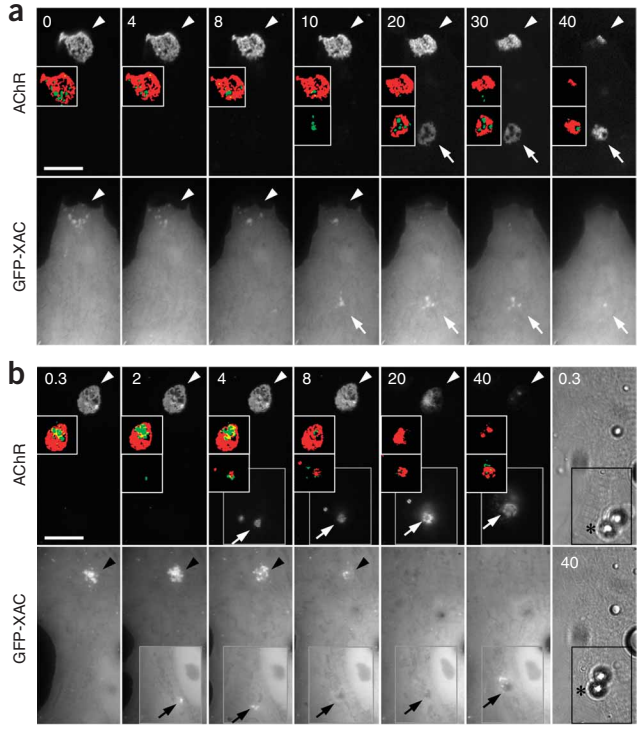

Figure 2 Dynamics of ADF/cofilin in spontaneous and agrin-induced redistribution of AChRs. (**a**) A time-lapse series showing the dynamic redistribution of GFP-XAC and AChRs in two spontaneous clusters. AChRs were labeled with Rh-BTX before the start of recordings. For better clarity, pseudo-colored images after an intensity threshold are shown in the insets. Arrowheads indicate the position of the original spontaneous cluster, and arrows indicate the position of a newly formed spontaneous cluster. Numbers indicate the elapsed time (measured in **h**) in the recordings. (**b**) A time-lapse series showing the dynamics of GFP-XAC in the formation and dispersal of agrin-induced and spontaneous AChR clusters, respectively. Muscle cells were labeled with Rh-BTX and then stimulated by agrin beads at 0 h. Pairs of pseudo-colored images after the intensity threshold are shown in the insets. Gray boxed regions were focused on the top of muscle cells where agrin beads made contacts with the muscle membrane. DIC images from the start and end of the recordings are included in the last column and show a slight lateral movement of beads (asterisks) on the muscle surface during the 40-h time-lapse recordings. Arrowheads indicate the position of the spontaneous cluster, and arrows indicate the position of the bead-induced specialization. Numbers indicate the elapsed time (measured in h) after bead stimulation. Scale bars represent 20 μm.

in muscle cells under agrin-bead stimulation. In this case, GFP-XAC became localized at the bead contact site as early as 2 h after stimulation, whereas no AChR clusters were detected at the same site until 4 h (**Fig. 2b**). Concurrently, we observed a substantial loss of GFP-XAC signals in the spontaneous AChR clusters at 8 h, which later dispersed gradually. Pseudo-color AChR and XAC signals clearly showed that the redistribution of AChRs was preceded by that of XAC from the spontaneous clusters to the bead-induced site. By monitoring six individual agrin bead-induced clusters at a higher temporal resolution (one frame every 15 min for 4 h after bead stimulation), we detected the formation of GFP-XAC puncta before that of AChR clusters at five out of six bead-induced sites, whereas in only one case did we detect both GFP-XAC and AChR clusters at the same time. The times taken after bead stimulation for the detection of GFP-XAC and AChR clusters were 77.5 ± 16.2 (s.e.m.) min and 110 ± 18 (s.e.m.) min, respectively (**Supplementary Fig. 6** online). The appearance of XAC at agrin-bead contacts and its disappearance at the spontaneous AChR clusters had a reciprocal temporal correlation that coincided with the formation of new AChR clusters and the dispersal of old ones (**Supplementary Fig. 6**). Therefore, XAC localization in the nascent postsynaptic sites induced by agrin might direct the formation of AChR clusters, and the maintenance of spontaneous AChR clusters may also require localized XAC.

Localized ADF/cofilin increases actin dynamic turnover

One potential function for locally concentrated XAC is to regulate the actin dynamics. When labeled with fluorescent phalloidin, filamentous actin (F-actin, total) was found at the perforations in the spontaneous AChR clusters (**Fig. 3a**), but actin-enriched myofibrils obscured the details concerning its association with AChR clusters. To selectively label newly formed F-actin, we masked existing F-actin with a membrane-permeable actin-binding drug, jasplakinolide[13], which competes with phalloidin for F-actin binding[24]. When jasplakinolide-treated muscle cells were allowed to recover in drug-free medium for 4 h, fluorescent phalloidin signals were largely diminished in myofibrils but were enriched at the cell peripheral and the AChR-poor perforations in the spontaneous clusters, suggesting that new F-actin was preferentially generated at these locations over the 4-h period.

We next labeled F-actin barbed ends by exposing the cells to rhodamine-actin in the mild detergent saponin[25]. We consistently found actin barbed ends concentrated at AChR-poor perforations in the spontaneous AChR clusters (**Fig. 3a**). The close relationship between XAC and actin barbed ends was reflected by its high colocalization coefficient in the triple staining of AChR, XAC and actin barbed ends (**Supplementary Fig. 7** online). We also labeled the monomeric globular actin (G-actin) with vitamin D–binding proteins[26] and found local enrichment of endogenous G-actin at those perforations in AChR clusters (**Fig. 3a**). These results suggest that the actin cytoskeleton in the perforated regions of spontaneous AChR clusters undergoes dynamic turnover. We tested this hypothesis by photo-activation and live imaging of muscle cells expressing photo-activatable GFP–actin (paGFP-actin)[27]. When the muscle cell was globally exposed to an ultraviolet light, paGFP-actin fluorescence illuminated myofibrils of the entire cells (**Fig. 3b**), demonstrating the effective photo-activation. On local activation around spontaneous AChR clusters, paGFP-actin fluorescence declined much faster in the perforated region than in the AChR area (**Fig. 3c**), suggesting a faster turnover rate for F-actin at these sites (**Fig. 3d** and **Supplementary Video 1** online). Similarly, we found that actin barbed ends and G-actin were distributed in a ring pattern surrounding the bead-induced AChR clusters (**Fig. 3e**). Photo-activation/imaging of paGFP-actin also showed a higher turnover rate for the actin cytoskeleton adjacent to the AChR clusters (**Fig. 3f,g** and **Supplementary Video 2** online). These observations indicate that XAC-associated dynamic actin remodeling is probably involved in spatial targeting of AChRs, rather than in anchoring and stabilization of surface receptors.

Vesicular AChRs accumulate at ADF/cofilin localization

To determine whether XAC-mediated actin dynamics are involved in vesicular trafficking of AChRs, we first used FM4-64 staining to probe membrane recycling[28]. We found that FM4-64 signals appeared as puncta in the AChR-poor perforations of the spontaneous clusters (**Fig. 4a**). Immunostaining of EEA1, an early endosomal marker[29], also showed local enrichment of endosomal vesicles in those perforations. We also found that, similar to XAC, FM4-64–labeled puncta and EEA1 signals accumulated around the agrin bead–induced AChR clusters

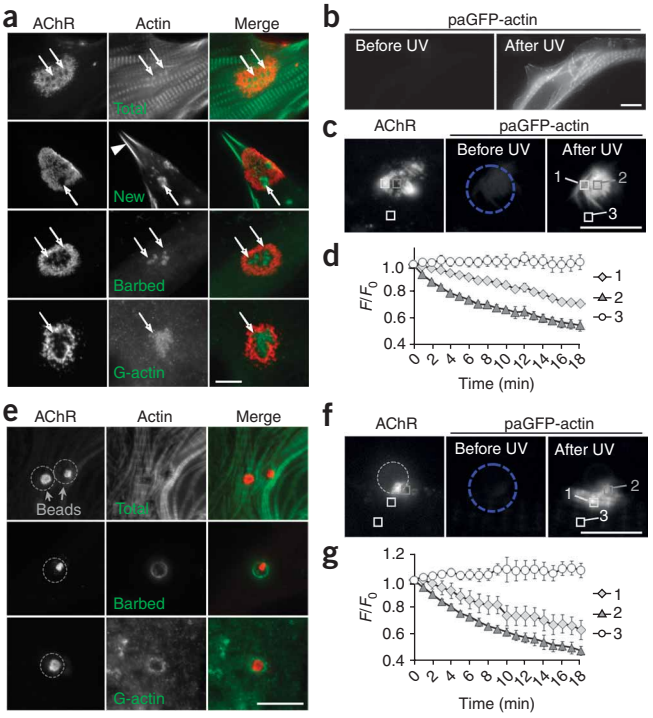

Figure 3 Regulation of actin dynamics by ADF/cofilin in spontaneous and synaptic AChR clusters. (**a**) Actin dynamics in the spontaneous AChR clusters as studied by dissecting different forms of F-actin: total F-actin, newly polymerized F-actin, actin barbed ends and G-actin (top to bottom rows). Arrows indicate enrichment of F-actin in the AChR clusters and the arrowhead marks the cell periphery. (**b**–**d**) Actin dynamics as revealed by paGFP-actin photoactivation. A cultured muscle cell expressing paGFP-actin was globally stimulated by ultraviolet (UV) light, resulting in a marked increase in paGFP-actin fluorescence intensity in the whole cell (**b**). When paGFP-actin was locally activated at a region (blue circle) containing the spontaneous AChR clusters in a muscle cell (**c**), fluorescent time-lapse imaging on photoactivated paGFP-actin revealed different rates of changes in fluorescence over time at three different regions, as presented in the intensity plot (**d**, $n = 4$). Analysis boxes: 1, AChR-rich region; 2, AChR-poor perforations; 3, background. (**e**) Spatial distribution of different forms of actin cytoskeleton in cultured muscle cells stimulated with agrin beads for 4 h. (**f**,**g**) Fluorescent images of paGFP-actin photoactivated in a region (blue circle) enclosing the bead-muscle contact (gray circle) in a muscle cell (**f**). The changes in fluorescence intensity of photoactivated paGFP-actin at three different regions are shown in the intensity plot (**g**, $n = 4$). paGFP-actin signals in a region adjacent to the bead-induced AChR clusters were found on a different focal plane with that associated with AChR clusters, thus we used paGFP-actin in the striation structure for comparison. Analysis boxes: 1, striation region; 2, region adjacent to the bead-induced AChR clusters; 3, background. Scale bars represent 10 μm. Error bars in **d** and **g** represent s.e.m.

(**Fig. 4b**). To test whether membrane recycling is involved in AChR clustering, we applied phenylarsine oxide, a general inhibitor of receptor-mediated endocytosis[30], and found that it abolished both the formation of agrin-induced AChR clusters and the dispersal of spontaneous AChR clusters (**Supplementary Fig. 8** online). Because phenylarsine oxide also inhibits tyrosine phosphatases[31], we employed low-temperature (4 °C) treatment to inhibit membrane fusion and vesicular trafficking[32]. Notably, the low temperature inhibited the redistribution of AChR, but not XAC, induced by the agrin bead. Finally, monodansylcadaverine, a clathrin-dependent endocytosis inhibitor[33], had no effect on agrin-induced localization of XAC and AChR (**Supplementary Fig. 8**). These findings suggest that spatially localized XAC may regulate actin dynamics to control the vesicular trafficking of AChRs in clathrin-independent mechanisms.

We next examined the presence of an internal pool of AChRs and its contribution to the surface AChRs using a double-labeling approach (see Online Methods and **Supplementary Fig. 9** online). We detected a substantial pool of internal AChRs associated with the spontaneous AChR clusters. Notably, these intracellular AChRs appeared as discrete puncta at the center of the AChR-poor perforations of the spontaneous clusters (**Fig. 4c**). The spatial segregation of surface and internal pools of AChRs was clearly depicted in a three-dimensional intensity profile. We also applied the same approach to examine agrin-induced AChR clusters and detected internal AChRs accumulated at the periphery surrounding the surface AChR clusters (**Fig. 4d**).

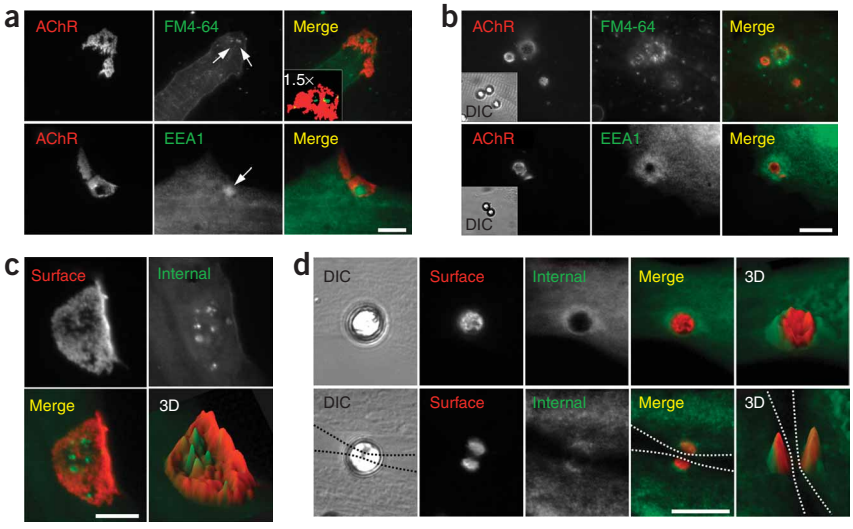

Figure 4 Local enrichment of vesicular trafficking machinery and intracellular AChRs in spontaneous and agrin-induced AChR clusters. (**a**) Vesicular components in spontaneous AChR clusters as labeled with FM4-64 in live cells or antibodies to EEA1 in fixed cultures. Pseudo-colored FM4-64 signals are highlighted and magnified in the inset. In the case of double staining with FM4-64, which emits red fluorescence, we used Alexa 488–BTX for AChRs. For the purpose of consistency, we reverted the colors such that FM4-64 is shown as green and AChRs as red. (**b**) Vesicular components surrounding the agrin bead–induced AChR clusters. After 4-h agrin-bead stimulation, the muscle cells were stained with either FM4-64 or antibodies to EEA1. Insets, DIC images showing the locations of bead-muscle contacts. (**c**,**d**) Surface and internal AChRs as revealed by differential double labeling. Cultured muscle cells were stimulated without (**c**) or with (**d**) agrin beads for 4 h. Surface AChRs were labeled with Rh-BTX and then saturated with unlabeled BTX. The cells were fixed, permeabilized, and the intracellular pool of AChRs (internal) was labeled with Alexa 488–BTX. Dotted lines represent the periphery of the cells where an agrin bead landed between two muscle cells. The spatial segregation of surface and internal pools of AChRs can be seen in the three-dimensional (3D) intensity plots of their fluorescence intensities in the last column of each panel. Scale bars represent 20 μm (**a**) and 10 μm (**b**–**d**).

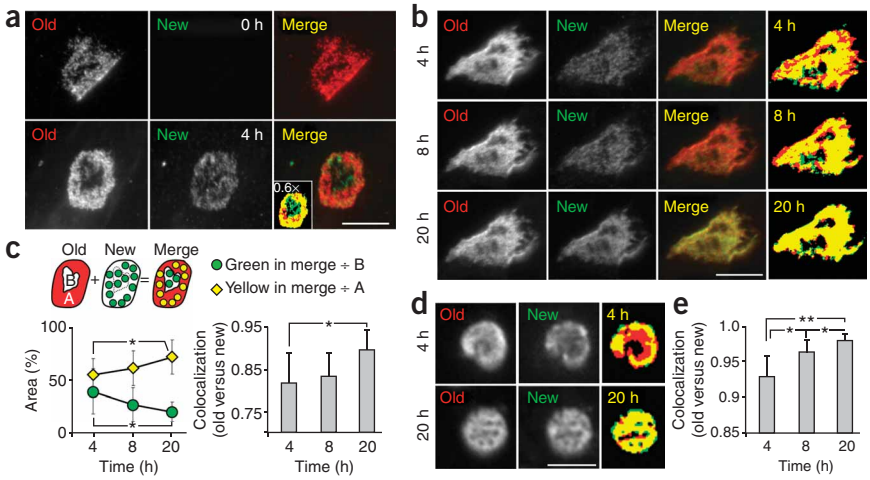

Figure 5 Time-dependent incorporation of newly inserted AChRs into the existing surface AChR clusters. (**a**) Existing and new AChRs as revealed by sequential double labeling. The existing AChRs (old) were labeled with Rh-BTX and then stained with a saturating dose of unlabeled BTX. After 0 h or 4 h, newly inserted AChRs (new) were labeled with Alexa 488–BTX. Inset, a merged image of old and new AChRs highlighted by pseudo-colors after an intensity threshold. (**b**) Paired images showing old and new AChRs at multiple time points after the sequential double labeling. (**c**) Quantification of the time-dependent incorporation of new AChRs into the old AChR clusters. A, area of the old AChR clusters; B, AChR-poor perforated regions in the clusters. We plotted the percentage of the area with new AChRs at the perforated region (green in merge divided by B) and the percentage of the area with new AChR insertion and/or incorporation into the existing AChR region (yellow in merge divided by A). The Pearson's colocalization coefficients between old and new AChR clusters at different time points were plotted. (**d**) Representative images showing old and new AChR clusters at the agrin bead contact. Paired images of old and new AChR clusters were taken at 4 h and 20 h. (**e**) Pearson's colocalization coefficients between old and new AChR clusters at multiple time points were plotted. Asterisks indicate significant differences (*t* test, * $P < 0.005$, ** $P < 0.001$). Scale bars represent 20 μm (**a**,**b**) and 5 μm (**d**). Error bars in **c** and **e** represent s.e.m.

Because XAC, dynamic actin, vesicular compartments and intracellular AChRs are colocalized, we suspected that new AChRs are inserted to the surface at these locations. To test this, we sequentially labeled the existing surface AChRs (old) with Rh-BTX and newly inserted AChRs (new) with Alexa 488–BTX (see Online Methods and **Supplementary Fig. 9**). If the second labeling occurred immediately after the first one, no signal was detected for new AChRs (**Fig. 5a**). If we performed the second labeling 4 h after the first, new AChRs were detected at both AChR-poor perforations and AChR-rich regions (**Fig. 5a**). The mix of new and old AChRs might result from the initial insertion of new AChRs into the AChR-poor perforations, followed by rapid redistribution and incorporation into the existing pools. To test this, we repeated the procedure but imaged both old and new AChRs at additional time points. The initial pair of images at 4 h showed a substantial portion of new AChRs that did not overlap with the old ones but became intermingled over time (**Fig. 5b**). We quantified the size of new AChRs in the perforations and normalized it against the total perforation area (**Fig. 5c**). The incorporation and/or insertion of new AChRs into old AChR clusters was similarly quantified and normalized against the total old AChR clusters. We found that the amount of new AChRs in the perforations of the clusters decreased from 4 h to 20 h, which was accompanied by a gradual increase in the incorporation and/or insertion of new AChRs into the old AChR clusters. In addition, the Pearson's colocalization coefficient between these two pools of surface AChRs had markedly increased over time. We further tested whether old and new AChRs induced by agrin beads are spatially segregated using the same approach. We found that newly inserted AChRs over the first 4-h agrin-bead stimulation were mainly localized at the periphery of the old AChR clusters; however, these two pools of AChRs became mixed by 20 h (**Fig. 5d**). The time-dependent colocalization of old and new AChRs induced by agrin beads was supported by an increase in the Pearson's colocalization coefficient (**Fig. 5e**). These data suggest that a substantial amount of new AChRs are inserted at the XAC-enriched AChR-poor regions in the spontaneous and agrin-induced clusters, which become gradually incorporated into the existing pool of AChRs.

ADF/cofilin regulates synaptic development

The depolymerizing/severing activity of ADF/cofilin is regulated by the phosphorylation state of its serine-3 residue[17], which can be mutated for overexpression to interfere with the endogenous ADF/cofilin

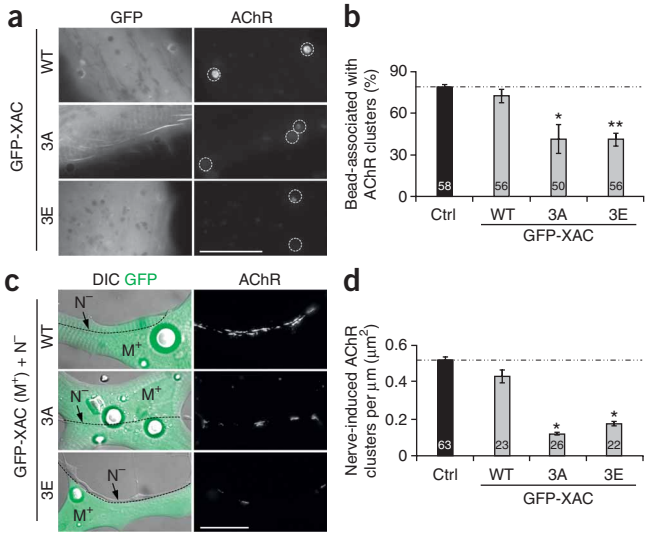

Figure 6 Regulation of agrin- and nerve-induced AChR clustering by ADF/cofilin activity. (**a**–**d**) Cultured muscle cells overexpressing either wild-type or mutant serine-3 phosphorylation forms of GFP-XAC were stimulated with agrin beads (**a**,**b**) or spinal neurons (**c**,**d**). (**a**) A representative set of images showing AChR clusters induced by 4-h agrin-bead stimulation in GFP-expressing muscle cells. Locations of agrin beads are outlined with dotted circles. (**b**) Quantification of the effects of XAC activity on agrin-induced AChR clustering. The percentage of agrin beads in association with those markers were scored if the respective markers were enriched at or around the bead contact sites. (**c**) A representative set of images showing AChR clustering on GFP-XAC–expressed muscles (M^+) induced by coculturing with wild-type spinal neurons (N^-) for 1 d. The nerve-muscle contacts are outlined with dotted lines for clarity. (**d**) Quantification of the effects of XAC activity on nerve-induced AChR clustering by plotting the area of nerve-induced AChR clusters per a unit length of nerve-muscle contact. Numbers indicate the number of bead-muscle contacts (**b**) or nerve-muscle contacts (**d**) counted from at least three independent experiments. Asterisks indicate significant differences (*t* test, * $P < 0.005$, ** $P < 0.001$). Scale bars represent 20 μm. Error bars in **b** and **d** represent s.e.m.

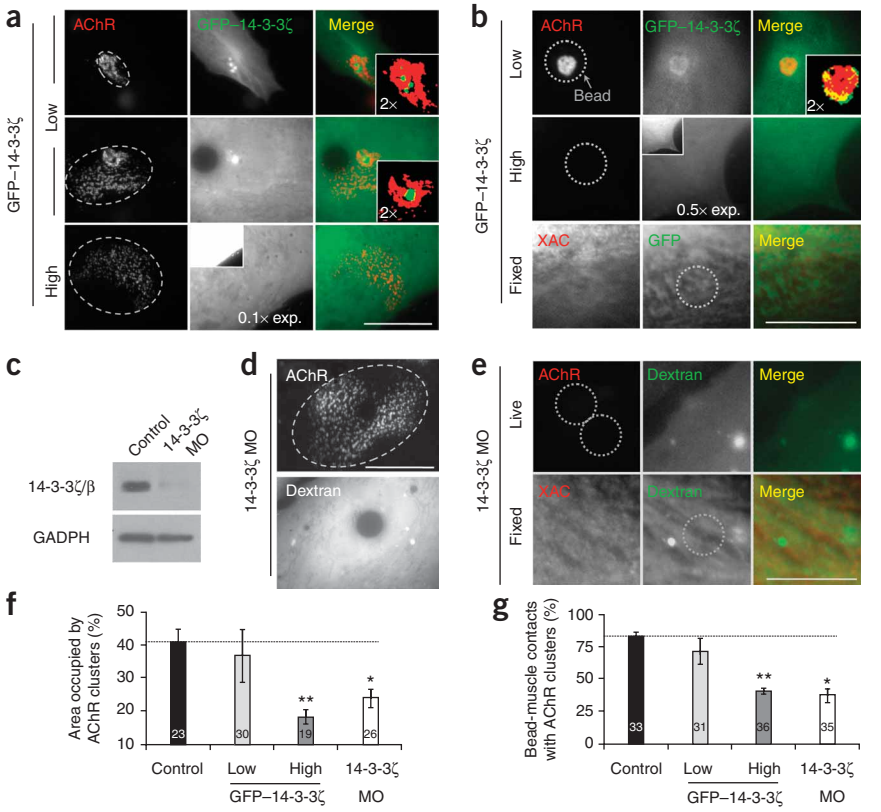

Figure 7 Involvement of 14-3-3ζ in AChR clustering and ADF/cofilin localization. (**a**,**b**) Representative sets of images showing the effects of different levels of GFP–14-3-3ζ overexpression on spontaneous (**a**) and agrin bead–induced (**b**) AChR clusters. The images of cells expressing high levels of GFP–14-3-3ζ were taken using a reduced exposure to allow for the examination of subcellular localization. The insets represent the images of the same cells but were acquired using the same exposure as that for cells expressing a low level of GFP–14-3-3ζ. One can thus appreciate the huge difference in the expression level of GFP–14-3-3ζ between these two groups. The magnified regions were pseudo-colored after an intensity threshold to show the differential localization of GFP–14-3-3ζ and AChRs (color insets). XAC immunostaining was performed in GFP–14-3-3ζ–expressing muscle cells stimulated with agrin beads. (**c**) Western blotting analysis of the 14-3-3ζ/β protein levels in the 14-3-3ζ morpholino (MO) knockdown experiment with GADPH as a loading control (full-length blots are presented in **Supplementary Fig. 12** online). (**d**) A similar disorganization of the spontaneous AChR clusters cultured from 14-3-3ζ morpholino embryos, as identified by fluorescent dextran signals. Ellipses (**a**,**d**) were drawn to outline the periphery of AChR clusters for the quantitative analysis in **f**. (**e**) A representative set of images showing the effects of 14-3-3ζ morpholino on AChR clustering and XAC localization induced by agrin beads. (**f**,**g**) Quantifications of spontaneous (**f**) and agrin bead–induced (**g**) AChR clusters in response to 14-3-3ζ overexpression or morpholino knockdown. Numbers indicate the number of samples counted from two independent experiments. Asterisks indicate significant differences (*t* test, * $P < 0.005$, ** $P < 0.001$). Scale bars represent 20 μm (**a**,**d**) and 10 μm (**b**,**e**). Error bars in **f** and **g** represent s.e.m.

activity. The effects of these XAC mutants on actin polymerization during neurite outgrowth have been previously characterized in cultured cortical neurons[34]. We found that overexpression of the 3A (constitutively active) or 3E (inactive) form of GFP-XAC, but not of wild type, reduced AChR clusters at the agrin bead contacts (**Fig. 6a**,**b**). Similarly, we found that muscle cells expressing GFP-XAC showed extensive AChR clusters along the nerve-contacted trails, which was markedly reduced by overexpression of XAC-3A or XAC-3E (**Fig. 6c**). The area of AChR clusters per unit length of nerve-muscle contact was largely reduced in muscle cells overexpressing GFP-XAC in 3A or 3E form when compared with cells overexpressing the wild-type form or control muscle cells (**Fig. 6d**).

We next performed whole-cell patch-clamp recordings of spontaneous synaptic currents (SSCs) in neuron-muscle cocultures[35]. In cocultures of muscle cells expressing different forms of GFP-XAC and wild-type spinal neurons, we found that expression of XAC-3A and XAC-3E in muscle cells reduced SSCs (**Supplementary Fig. 10** online). The decrease in the SSC amplitude was consistent with the reduced AChRs that we found along the nerve-muscle contacts after the expression of XAC-3A or XAC-3E. The reduction in the frequency of SSCs by XAC-3E expression might result from XAC-3E inhibition of retrograde signaling that affects presynaptic transmitter release. Nonetheless, these data provide evidence that ADF/cofilin phosphocycling on the serine-3 residue regulates AChR clustering and synaptic function.

14-3-3 mediates XAC localization and AChR clustering

The 14-3-3 family of phosphoproteins is known for its scaffolding role in subcellular targeting of intracellular signals[36]. Among at least seven mammalian isoforms, ADF/cofilin interacts with 14-3-3ζ and 14-3-3ε *in vitro*[37]. We expressed GFP–14-3-3ζ in muscle cells and examined its distribution and effects on AChR clustering. When GFP–14-3-3ζ was expressed at a low level, it was enriched at the perforated regions in the spontaneous AChR clusters (**Fig. 7a**). In some cases, we observed largely scattered AChR clusters, but with a small region of concentrated AChRs, at which GFP-14-3-3ζ was only found to localize to the small concentrated AChR area. At a high level of GFP–14-3-3ζ expression, however, most of the spontaneous AChR clusters showed a scattered pattern without preferential localization of GFP–14-3-3ζ. Similar effects of GFP–14-3-3ζ overexpression on agrin bead–induced AChR clustering were also observed (**Fig. 7b**). Notably, GFP–14-3-3ζ overexpression also diminished XAC localization in agrin bead–muscle contacts.

To further investigate the role of 14-3-3ζ in ADF/cofilin localization and AChR clustering, we knocked down *Xenopus* 14-3-3ζ expression by morpholino antisense oligonucleotides. The effectiveness of 14-3-3ζ morpholino knockdown was confirmed by western blotting using an antibody to *Xenopus* 14-3-3ζ/β (**Fig. 7c**). In muscle cells expressing 14-3-3ζ morpholino (as evidenced by fluorescent dextran signals), we found that the spontaneous AChR clusters were also scattered as small aggregates (**Fig. 7d**). Consistently, morpholino knockdown of 14-3-3ζ also blocked AChR clustering and XAC localization induced by agrin beads (**Fig. 7e**). Quantitative analysis showed that either overexpression of GFP–14-3-3ζ at a high level or knockdown of endogenous 14-3-3ζ expression in muscle cells disrupted the compact pattern of the spontaneous AChR clusters and reduced the percentage of AChR-occupied area (**Fig. 7f**). Similarly, AChR clustering induced by agrin beads was also attenuated (**Fig. 7g**).

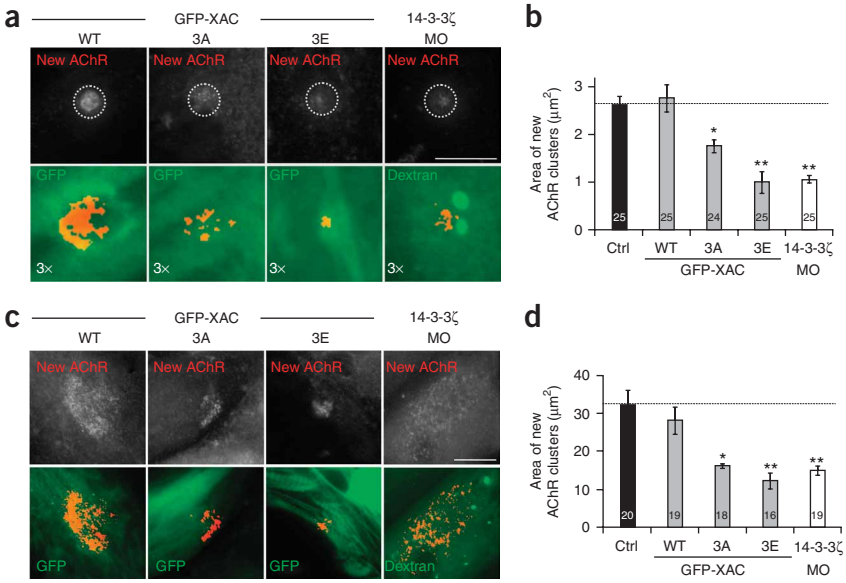

Figure 8 Regulation of surface targeting of new AChRs by ADF/cofilin activity and 14-3-3ζ. (**a**,**c**) Representative images showing newly inserted AChRs in agrin bead–induced (**a**) or spontaneous (**c**) AChR clusters in muscle cells expressing different XAC mutants or 14-3-3ζ morpholino knockdown. The pre-existing surface AChRs were first masked with a saturating dose of unlabeled BTX. After 4 h, the cells were labeled with Rh-BTX and fixed to allow precise and reliable quantification of the newly inserted AChRs (new AChR) in a large number of cells at this particular time point. The muscle cells overexpressing wild-type or mutant GFP-XAC were identified by GFP expression, whereas 14-3-3ζ morpholino knockdown was identified by fluorescent dextran signals. It should be noted that the exact subcellular localization of GFP-tagged proteins may be altered after fixation. The area of new AChRs was highlighted with red pseudo-colors through the application of an intensity threshold in merge images (bottom rows). The locations of agrin beads are outlined with dotted circles in top panels. (**b**,**d**) Quantifications of XAC activity and 14-3-3ζ manipulations on surface targeting of new AChRs in agrin-induced (**b**) or spontaneous clusters (**d**). Areas of new AChR clusters at the bead-muscle contacts and at the spontaneous clusters were measured in the threshold images. Numbers indicate the number of bead-muscle contacts (**b**) or spontaneous clusters (**d**) measured from two independent experiments. Asterisks indicate significant differences (*t* test, * $P < 0.005$, ** $P < 0.001$). Error bars in **b** and **d** represent s.e.m.

These results thus suggest that 14-3-3ζ is involved in the spatial localization of ADF/cofilin for AChR clustering.

To better understand the relationship between ADF/cofilin localization and surface targeting of AChRs, we tested whether manipulation of either ADF/cofilin activity (by overexpression of XAC mutants) or its localization (by 14-3-3ζ morpholino knockdown) affects the surface insertion of new AChRs. Because of the technical limit for triple staining, we masked all surface AChRs on the muscle cells with a saturating dose of unlabeled BTX (see **Fig. 5a** for the masking effectiveness). After a 4-h agrin-bead stimulation, the muscle cells were labeled with Rh-BTX and subsequently fixed for visualization and quantification of newly inserted AChRs. We found that overexpression of GFP-XAC had no influence on surface insertion of new AChRs induced by agrin beads. In muscle cells expressing XAC mutants or 14-3-3ζ morpholino, however, the amount of new AChR clusters was markedly reduced at the bead-induced sites (**Fig. 8a**,**b**). Similarly, AChR insertion to the membrane surface at the spontaneous clusters was also attenuated by the overexpression of XAC mutants or 14-3-3ζ morpholino knockdown (**Fig. 8c**,**d**). Therefore, disruption of ADF/cofilin localization or activity impairs AChR surface insertion.

DISCUSSION

Regulated trafficking of postsynaptic receptors represents a major mechanism underlying synaptic plasticity[1,3], but the cytoskeletal involvement is not well understood. We found that spatiotemporally restricted ADF/cofilin-mediated actin dynamics regulate the trafficking and surface targeting of AChRs to the nascent postsynaptic sites at developing NMJs. Our findings indicate that, on top of the passive diffusion-trap mechanism, an active receptor-trafficking mechanism may underlie the redistribution of AChRs from the spontaneous clusters to the nascent postsynaptic sites during synaptogenic stimulation. We hypothesize that, on synaptogenic induction, AChRs are endocytosed from the spontaneous AChR clusters, which, together with the new synthesized AChRs, may be transported and delivered to the nascent postsynaptic sites for insertion. During this process, ADF/cofilin may be among the first to localize to the nascent sites (through 14-3-3 scaffolding activated by synaptogenic signals) to modulate local dynamic actin cytoskeleton that defines, assists and/or maintains vesicular fusion and recycling of AChRs (see **Supplementary Fig. 11** online).

F-actin is considered to be a cytoskeletal scaffold for the docking and anchorage of structural and signaling molecules to the postsynaptic sites at NMJs[14,38]. Our data here have elucidated a previously unknown function for ADF/cofilin-mediated actin dynamics in spatiotemporal regulation of AChR trafficking and clustering. The enrichment of new F-actin, actin barbed ends and G-actin in locations adjacent to, but not overlapping with, surface AChR clusters in the spontaneous and synaptic specializations argue against the idea that ADF/cofilin-mediated actin dynamics function as a stable scaffold for receptor anchorage and immobilization. The colocalization of these dynamic actin regions with the vesicular pool of internal AChRs, together with the presence of newly inserted surface AChRs in these regions, indicates that spatially restricted dynamic actin may actively regulate the vesicular trafficking of AChRs to and from the membrane. Dynamic actin turnover has been known to regulate vesicular membrane trafficking[39,40]. Local increased dynamic actin turnover by ADF/cofilin may break the cortical actin barrier and/or actively facilitate the vesicle fusion to the plasma membrane. The permissive and active roles for dynamic actin in vesicular trafficking of AChRs are not exclusive and may cooperate for spatial control of AChR delivery to the postsynaptic site. Notably, we observed a compact cluster of ADF/cofilin at early time points after agrin-bead stimulation, when AChR clusters had not yet been formed, which subsequently was transformed into a ring structure surrounding AChR clusters. Similar to the central synapses[2], it is conceivable that ADF/cofilin-mediated vesicular trafficking (especially the exocytosis) of postsynaptic receptors is restricted at the receptor-poor perisynaptic sites for effective modulation of postsynaptic receptor density.

Recent studies suggest that a high concentration of active cofilin favors F-actin nucleation[41,42]. The localization of active,

nonphosphorylated ADF/cofilin at sites of newly polymerized F-actin with elevated levels of barbed ends and endogenous G-actin suggests that ADF/cofilin may sever the existing F-actin and contribute to the abundant supply of actin monomers and barbed ends for rapid actin assembly in the spontaneous and synaptic AChR clusters. The suppression of AChR clustering by overexpression of either constitutively active or inactive ADF/cofilin indicates that phosphocycling-dependent regulation of localized ADF/cofilin is required for its function in altering the actin cytoskeleton for AChR trafficking. This can also be explained by a 'set-point' hypothesis, whereby hyper- or hypo-activity of ADF/cofilin may imbalance the actin dynamics and the proper trafficking of AChRs to the postsynaptic membrane. Moreover, the finding that constitutively active GFP–XAC-3A accumulates in the perforations of spontaneous AChR clusters (**Supplementary Fig. 2**), but not in agrin-induced AChR clusters (**Fig. 6a**), indicates that disruption of ADF/cofilin phosphocycling may also impair its translocation in response to agrin signaling. Previous studies have shown that agrin-MuSK signaling involves p21-activated kinase[43], an activator of LIM kinases[44]. LIM kinases are the major kinases that phosphorylate and inactivate ADF/cofilin[45]. It is thus reasonable to speculate that both ADF/cofilin activity and translocation may be regulated by phosphocycling, which may be targeted by agrin-MuSK signaling.

Our data also indicate that the 14-3-3 family of scaffolding proteins is involved in ADF/cofilin localization. Both serine-3 phosphorylated and nonphosphorylated ADF/cofilin binds to 14-3-3, although the former has a higher affinity. Moreover, phosphorylation on the serine-23 or serine-24 residue of ADF/cofilin appears to be sufficient for its 14-3-3 binding[37]. Therefore, ADF/cofilin localization via 14-3-3 molecules does not necessarily depend on its activity. At present, only 14-3-3ζ and 14-3-3ε have been reported to interact with ADF/cofilin *in vitro*[37,46], but other isoforms may interact with ADF/cofilin because of the high homology of 14-3-3 family members[47]. Notably, 14-3-3γ colocalizes and potentially interacts with MuSK at adult NMJs[48]. Whether 14-3-3γ regulates ADF/cofilin localization for actin-dependent AChR trafficking remains to be investigated. Besides interacting directly with ADF/cofilin, 14-3-3 also interacts with the upstream regulators of ADF/cofilin, LIM kinase[46] and Slingshot phosphatase[45]. Collectively, 14-3-3 may spatially localize both ADF/cofilin and its regulators to the synaptic sites to coordinately control the dynamic actin turnover for AChR trafficking. Finally, additional synapse-specific scaffolding proteins may also participate in ADF/cofilin localization.

In conclusion, our study has identified a previously unknown function for ADF/cofilin in postsynaptic receptor trafficking and clustering. Our findings indicate that ADF/cofilin may spatiotemporally regulate the trafficking and surface delivery of AChRs during neuromuscular synaptogenesis. ADF/cofilin is also concentrated at the periphery of the postsynaptic density at the central synapses[49] and is involved in the trafficking of growth factor receptors in invasive tumor cells[50]. Therefore, we can speculate that ADF/cofilin-mediated actin dynamics may be important in receptor trafficking that underlies a broad range of cell functions.

METHODS

Methods and any associated references are available in the online version of the paper at http://www.nature.com/natureneuroscience/.

Note: Supplementary information is available on the Nature Neuroscience website.

ACKNOWLEDGMENTS

We would like to thank B. Lu (National Institute of Child Health and Human Development) for his help in our electrophysiological experiments. This work is supported by grants from National Institutes of Health to J.Q.Z. (GM083889 and AG029596) and J.R.B. (NS40371). C.W.L. was supported by a postdoctoral fellowship from The Croucher Foundation.

AUTHOR CONTRIBUTIONS

C.W.L. designed and performed most of the experiments, data analyses and manuscript writing. J.H. did the electrophysiological recording. J.R.B. provided insightful advice to the experiments and critical input to the manuscript and contributed the reagents for ADF/cofilin and 14-3-3ζ. L.H. and R.L. performed the molecular subcloning of some of the DNA constructs that were used. J.Q.Z. formulated and oversaw the research project and directed the experiments, analyses and writing.

Published online at http://www.nature.com/natureneuroscience/
Reprints and permissions information is available online at http://www.nature.com/reprintsandpermissions/

1. Bredt, D.S. & Nicoll, R.A. AMPA receptor trafficking at excitatory synapses. *Neuron* **40**, 361–379 (2003).
2. Kennedy, M.J. & Ehlers, M.D. Organelles and trafficking machinery for postsynaptic plasticity. *Annu. Rev. Neurosci.* **29**, 325–362 (2006).
3. Song, I. & Huganir, R.L. Regulation of AMPA receptors during synaptic plasticity. *Trends Neurosci.* **25**, 578–588 (2002).
4. Sanes, J.R. & Lichtman, J.W. Development of the vertebrate neuromuscular junction. *Annu. Rev. Neurosci.* **22**, 389–442 (1999).
5. Lin, W. *et al.* Distinct roles of nerve and muscle in postsynaptic differentiation of the neuromuscular synapse. *Nature* **410**, 1057–1064 (2001).
6. Sanes, J.R. & Lichtman, J.W. Induction, assembly, maturation and maintenance of a postsynaptic apparatus. *Nat. Rev. Neurosci.* **2**, 791–805 (2001).
7. Misgeld, T., Kummer, T.T., Lichtman, J.W. & Sanes, J.R. Agrin promotes synaptic differentiation by counteracting an inhibitory effect of neurotransmitter. *Proc. Natl. Acad. Sci. USA* **102**, 11088–11093 (2005).
8. DeChiara, T.M. *et al.* The receptor tyrosine kinase MuSK is required for neuromuscular junction formation *in vivo*. *Cell* **85**, 501–512 (1996).
9. Lin, W. *et al.* Neurotransmitter acetylcholine negatively regulates neuromuscular synapse formation by a Cdk5-dependent mechanism. *Neuron* **46**, 569–579 (2005).
10. Chen, F. *et al.* Rapsyn interaction with calpain stabilizes AChR clusters at the neuromuscular junction. *Neuron* **55**, 247–260 (2007).
11. Peng, H.B., Zhao, D.Y., Xie, M.Z., Shen, Z.W. & Jacobson, K. The role of lateral migration in the formation of acetylcholine receptor clusters induced by basic polypeptide-coated latex beads. *Dev. Biol.* **131**, 197–206 (1989).
12. Camus, G., Jasmin, B.J. & Cartaud, J. Polarized sorting of nicotinic acetylcholine receptors to the postsynaptic membrane in Torpedo electrocyte. *Eur. J. Neurosci.* **10**, 839–852 (1998).
13. Dai, Z., Luo, X., Xie, H. & Peng, H.B. The actin-driven movement and formation of acetylcholine receptor clusters. *J. Cell Biol.* **150**, 1321–1334 (2000).
14. Hall, Z.W., Lubit, B.W. & Schwartz, J.H. Cytoplasmic actin in postsynaptic structures at the neuromuscular junction. *J. Cell Biol.* **90**, 789–792 (1981).
15. Kummer, T.T., Misgeld, T., Lichtman, J.W. & Sanes, J.R. Nerve-independent formation of a topologically complex postsynaptic apparatus. *J. Cell Biol.* **164**, 1077–1087 (2004).
16. Peng, H.B., Baker, L.P. & Chen, Q. Tissue culture of *Xenopus* neurons and muscle cells as a model for studying synaptic induction. *Methods Cell Biol.* **36**, 511–526 (1991).
17. Bamburg, J.R. Proteins of the ADF/cofilin family: essential regulators of actin dynamics. *Annu. Rev. Cell Dev. Biol.* **15**, 185–230 (1999).
18. Shaw, A.E. *et al.* Cross-reactivity of antibodies to actin-depolymerizing factor/cofilin family proteins and identification of the major epitope recognized by a mammalian actin-depolymerizing factor/cofilin antibody. *Electrophoresis* **25**, 2611–2620 (2004).
19. Wen, Z. *et al.* BMP gradients steer nerve growth cones by a balancing act of LIM kinase and Slingshot phosphatase on ADF/cofilin. *J. Cell Biol.* **178**, 107–119 (2007).
20. Schindelholz, B. & Reber, B.F. Quantitative estimation of F-actin in single growth cones. *Methods* **18**, 487–492 (1999).
21. Bowe, M.A. & Fallon, J.R. The role of agrin in synapse formation. *Annu. Rev. Neurosci.* **18**, 443–462 (1995).
22. Daggett, D.F., Stone, D., Peng, H.B. & Nikolics, K. Full-length agrin isoform activities and binding site distributions on cultured *Xenopus* muscle cells. *Mol. Cell. Neurosci.* **7**, 75–88 (1996).
23. Kuromi, H. & Kidokoro, Y. Nerve disperses pre-existing acetylcholine receptor clusters prior to induction of receptor accumulation in *Xenopus* muscle cultures. *Dev. Biol.* **103**, 53–61 (1984).
24. Bubb, M.R., Senderowicz, A.M., Sausville, E.A., Duncan, K.L. & Korn, E.D. Jasplakinolide, a cytotoxic natural product, induces actin polymerization and competitively inhibits the binding of phalloidin to F-actin. *J. Biol. Chem.* **269**, 14869–14871 (1994).
25. Schafer, D.A. *et al.* Visualization and molecular analysis of actin assembly in living cells. *J. Cell Biol.* **143**, 1919–1930 (1998).
26. Cao, L.G., Fishkind, D.J. & Wang, Y.L. Localization and dynamics of nonfilamentous actin in cultured cells. *J. Cell Biol.* **123**, 173–181 (1993).
27. Patterson, G.H. & Lippincott-Schwartz, J. A photoactivatable GFP for selective photolabeling of proteins and cells. *Science* **297**, 1873–1877 (2002).

28. Cochilla, A.J., Angleson, J.K. & Betz, W.J. Monitoring secretory membrane with FM1–43 fluorescence. *Annu. Rev. Neurosci.* **22**, 1–10 (1999).
29. Mu, F.T. *et al.* EEA1, an early endosome–associated protein. EEA1 is a conserved alpha-helical peripheral membrane protein flanked by cysteine 'fingers' and contains a calmodulin-binding IQ motif. *J. Biol. Chem.* **270**, 13503–13511 (1995).
30. Hertel, C., Coulter, S.J. & Perkins, J.P. A comparison of catecholamine-induced internalization of beta-adrenergic receptors and receptor-mediated endocytosis of epidermal growth factor in human astrocytoma cells. Inhibition by phenylarsine oxide. *J. Biol. Chem.* **260**, 12547–12553 (1985).
31. Dai, Z. & Peng, H.B. A role of tyrosine phosphatase in acetylcholine receptor cluster dispersal and formation. *J. Cell Biol.* **141**, 1613–1624 (1998).
32. Tsuji, S. Electron-microscope cytochemistry of acetylcholine-like cation by means of low-temperature 'ionic fixation'. *Histochemistry* **81**, 453–455 (1984).
33. Schütze, S. *et al.* Inhibition of receptor internalization by monodansylcadaverine selectively blocks p55 tumor necrosis factor receptor death domain signaling. *J. Biol. Chem.* **274**, 10203–10212 (1999).
34. Meberg, P.J. & Bamburg, J.R. Increase in neurite outgrowth mediated by overexpression of actin depolymerizing factor. *J. Neurosci.* **20**, 2459–2469 (2000).
35. Evers, J., Laser, M., Sun, Y.A., Xie, Z.P. & Poo, M.M. Studies of nerve-muscle interactions in *Xenopus* cell culture: analysis of early synaptic currents. *J. Neurosci.* **9**, 1523–1539 (1989).
36. Fu, H., Subramanian, R.R. & Masters, S.C. 14-3-3 proteins: structure, function and regulation. *Annu. Rev. Pharmacol. Toxicol.* **40**, 617–647 (2000).
37. Gohla, A. & Bokoch, G.M. 14-3-3 regulates actin dynamics by stabilizing phosphorylated cofilin. *Curr. Biol.* **12**, 1704–1710 (2002).
38. Luther, P.W., Samuelsson, S.J., Bloch, R.J. & Pumplin, D.W. Cytoskeleton-membrane interactions at the postsynaptic density of *Xenopus* neuromuscular junctions. *J. Neurocytol.* **25**, 417–427 (1996).
39. Sokac, A.M. & Bement, W.M. Kiss-and-coat and compartment mixing: coupling exocytosis to signal generation and local actin assembly. *Mol. Biol. Cell* **17**, 1495–1502 (2006).
40. Eitzen, G. Actin remodeling to facilitate membrane fusion. *Biochim. Biophys. Acta* **1641**, 175–181 (2003).
41. Andrianantoandro, E. & Pollard, T.D. Mechanism of actin filament turnover by severing and nucleation at different concentrations of ADF/cofilin. *Mol. Cell* **24**, 13–23 (2006).
42. Chen, H. *et al. In vitro* activity differences between proteins of the ADF/cofilin family define two distinct subgroups. *Biochemistry* **43**, 7127–7142 (2004).
43. Luo, Z.G. *et al.* Regulation of AChR clustering by Dishevelled interacting with MuSK and PAK1. *Neuron* **35**, 489–505 (2002).
44. Edwards, D.C., Sanders, L.C., Bokoch, G.M. & Gill, G.N. Activation of LIM-kinase by Pak1 couples Rac/Cdc42 GTPase signaling to actin cytoskeletal dynamics. *Nat. Cell Biol.* **1**, 253–259 (1999).
45. Soosairajah, J. *et al.* Interplay between components of a novel LIM kinase-slingshot phosphatase complex regulates cofilin. *EMBO J.* **24**, 473–486 (2005).
46. Birkenfeld, J., Betz, H. & Roth, D. Identification of cofilin and LIM-domain-containing protein kinase 1 as novel interaction partners of 14-3-3 zeta. *Biochem. J.* **369**, 45–54 (2003).
47. Lau, J.M., Wu, C. & Muslin, A.J. Differential role of 14-3-3 family members in *Xenopus* development. *Dev. Dyn.* **235**, 1761–1776 (2006).
48. Strochlic, L. *et al.* 14-3-3 gamma associates with muscle specific kinase and regulates synaptic gene transcription at vertebrate neuromuscular synapse. *Proc. Natl. Acad. Sci. USA* **101**, 18189–18194 (2004).
49. Racz, B. & Weinberg, R.J. Spatial organization of cofilin in dendritic spines. *Neuroscience* **138**, 447–456 (2006).
50. Nishimura, Y., Yoshioka, K., Bernard, O., Bereczky, B. & Itoh, K. A role of LIM kinase 1/cofilin pathway in regulating endocytic trafficking of EGF receptor in human breast cancer cells. *Histochem. Cell Biol.* **126**, 627–638 (2006).

ONLINE METHODS

Microinjection and primary culture preparation from *Xenopus* embryos. DNA constructs encoding GFP-XAC wild type/3A/3E[34], GFP–14-3-3ζ or paGFP-actin were microinjected into one blastomere of two-cell stage *Xenopus* embryos. Typically, each embryo was injected with 20–100 pg of DNA. To knock down the expression of 14-3-3ζ, we injected custom-designed morpholino antisense oligonucleotides (5′-CTG GAC CAG TTC ATT TTT ATC CAT G-3′, Gene Tools) with the cell-lineage tracer Oregon Green 488–dextran (Invitrogen) into one- or two-cell stage embryos. GFP- or dextran-expressing embryos were screened for primary culture preparation. Myotomal muscle tissues and neural tubes were dissected from stage 19–22 *Xenopus* embryos after collagenase treatment as described previously[16]. Dissociated muscle cells were plated on glass coverslips coated with laminin-containing matrix, ECL (Millipore), and grown in culture medium containing 10% Leibovitz's L-15 medium (vol/vol; Invitrogen), 87% Steinberg's solution (vol/vol; 60 mM NaCl, 0.67 mM KCl, 0.35 mM $Ca(NO_3)_2$, 0.83 mM $MgSO_4$, 10 mM HEPES, pH 7.4), 1% fetal bovine serum (vol/vol), 1% penicillin/streptomycin (vol/vol) and 1% gentamicin sulfate (vol/vol). Unless specified, the muscle cultures were kept at ~18 °C for at least 5 d before experiments to minimize the presence of yolk granules. To make nerve-muscle cocultures, we plated dissociated spinal neurons on 5-d-old muscle cultures for the induction of synaptogenesis. All of the experiments involving *Xenopus* frogs and embryos were carried out in accordance with the US National Institutes of Health guidelines for animal use and were approved by the Institutional Animal Care and Use Committee of the University of Medicine and Dentistry of New Jersey Robert Wood Johnson Medical School and Emory University.

RT-PCR analysis of XAC expression in *Xenopus* myotomal muscle tissues. Dissociated muscle tissues from two *Xenopus* embryo at stage 19–22 were dissected and lysed for the synthesis of the first-strand cDNA by the SuperScript III Cells Direct cDNA Synthesis kit (Invitrogen). We used a pair of specific primers for the XAC sequence: 5′-TCT CTC AAA ACC ATA GGC ACT-3′ (forward) and 5′-ACA GGA ATT TCG ACA CCC TC-3′ (reverse). PCR products were resolved in ethidium bromide–stained agarose gels. We expected a band of PCR products at a molecular weight of 236 base pairs if XAC mRNA was present in the muscle tissues.

Visualization of newly polymerized F-actin, free actin barbed ends and G-actin. To visualize the newly polymerized F-actin, the less dynamic form of F-actin (enriched mainly in myofibrils) was masked with a cell-permeable actin-binding drug, jasplakinolide (Invitrogen), at 10 μM for 3 h in live muscle cells[13]. After recovery in drug-free medium, the treated cells were fixed, permeabilized, and the newly polymerized actin filaments were probed by fluorescein phalloidin (Invitrogen). Free F-actin barbed ends were labeled by 0.45 μM rhodamine-conjugated G-actin (Cytoskeleton) for 3 min in the saponin permeabilization solution (20 mM HEPES, 138 mM KCl, 4 mM $MgCl_2$, 3 mM EGTA, 0.2 mg ml^{-1} saponin, 1 mM ATP and 1% BSA (wt/vol), pH 7.5)[25]. The labeled cells were fixed with 2% paraformaldehyde (PFA, vol/vol) immediately after being labeled for imaging. Endogenous G-actin labeling was performed as previously described[26]. In short, muscle cells were fixed with 4% PFA for 10 min and then extracted in cold acetone for 5 min. The cells were incubated with 10 μg ml^{-1} of the vitamin D–binding protein DBP (Calbiochem) for 1 h, followed by a standard immunofluorescence protocol with a polyclonal antibody to DBP (Dako).

FM dye staining. To visualize constitutive vesicular recycling in muscle cells, we exposed the cells to 5 μg ml^{-1} FM4-64 (Invitrogen) in culture medium for 30 min. Labeled cells were washed twice with ice-cold calcium- and magnesium-free Hank's balanced salt solution (Invitrogen) and then examined live by fluorescence microscopy.

Identification of different pools of AChRs. To differentiate between surface and internal AChRs, we labeled surface AChRs with 0.1 μM rhodamine-conjugated BTX (Invitrogen) for 45 min and then added a saturating dose (6 μM) of unlabeled BTX (Invitrogen) for 15 min. The cells were fixed with 4% PFA and permeabilized with 0.5% Triton X-100 (vol/vol). After blocking with 5% BSA for 1 h, the internal pool of AChRs was labeled with 1 μM Alexa 488–conjugated BTX (Invitrogen) for 1 h. To differentiate between existing (old) and newly inserted (new) AChR clusters in live cultured muscle cells, we labeled old AChRs with 0.1 μM rhodamine–conjugated BTX and saturated them with 6 μM unlabeled BTX. After bead stimulation or recovery in culture medium, new AChRs were labeled with 1 μM Alexa 488–conjugated BTX for 45 min (a schematic illustration of these two labeling methods is provided in **Supplementary Fig. 9**).

Immunocytochemistry and immunoblotting. For immunofluorescent experiments, *Xenopus* muscle or nerve-muscle cultures were fixed with 4% PFA and 0.25% glutaraldehyde for 15 min and permeabilized with 0.5% Triton X-100 for 10 min. For immunostaining of pXAC, we increased the fixation time to 45 min to maximally preserve pXAC signals. The fixed cultures were blocked with 5% BSA for at least 1 h. They were then stained with primary antibodies for 2 h and with secondary antibodies for 45 min. The coverslips were mounted on slides with an anti-fade agent, Fluoromount-G (SouthernBiotech). For immunoblotting experiments, stage 19–22 *Xenopus* embryos were homogenized in the lysis buffer (50 mM Tris-HCl (pH 7.4), 150 mM NaCl, 1 mM EDTA, 1% Triton X-100, 1 mM phenylmethylsulfonyl fluoride, 1 mg ml^{-1} aprotinin, 1 mg ml^{-1} leupeptin and 1 mg ml^{-1} pepstatin). The protein lysates were resolved by 12% Tris-glycine pre-cast gels (Invitrogen) and transferred to nitrocellulose membranes, which were blocked in phosphate-buffered saline with 0.2% Tween-20 (vol/vol) and 10% milk (wt/vol) for 1 h and then immunoblotted with primary rabbit antibodies to 14-3-3ζ/β (Millipore) for 1 h. The primary antibodies were detected by horseradish peroxidase–conjugated secondary antibodies and enhanced chemiluminescence substrate. The membranes were stripped for 15 min with the Restore Plus Western Blot stripping buffer (Thermo) and re-probed with GADPH antibodies (Santa Cruz).

Fluorescence microscopy and time-lapse imaging. Fluorescent imaging was performed on an inverted microscope (TE2000, Nikon) using a 60 × N.A. 1.4 Plan Apo or a 100 × N.A. 1.3 Super Fluor (in photoactivation experiments) objective with identical settings between the control and experimental groups. Digital still or time-lapse images were captured with a CCD camera (SensiCam QE, Cooke Scientific) using the IPLab imaging software (BD Biosciences). Confocal imaging was carried out on a Nikon inverted microscope (TE300) equipped with a Nikon C1 confocal unit using a 60 × N.A.1.4 Plan Apo objective.

Electrophysiology. Dissociated muscle cells and spinal neurons were plated on plain glass coverslips. SSCs were recorded from innervated muscle cells in 1-d-old nerve-muscle cocultures by the whole-cell recording methods at 20–25 °C. The recording solution contained 140 mM NaCl, 5 mM KCl, 1 mM, $CaCl_2$, 1 mM $MgCl_2$ and 10 mM HEPES (pH 7.4). The intra-pipette solution contained 145 mM KCl, 1 mM NaCl, 1 mM $MgCl_2$, 1 mM Mg-ATP and 10 mM HEPES (pH 7.2). The membrane potentials of the muscle cells recorded were voltage clamped at –70 mV. All data were collected by an Axopatch 200B patch-clamp amplifier (Molecular Devices). The frequency of SSCs was defined as the number of SSC events per min. The amplitudes of SSCs were analyzed using the Strathclyde electrophysiology software (University of Strathclyde).

Data and statistical analyses. Data are reported as mean ± s.e.m. unless otherwise indicated. Quantitative measurement, three-dimensional intensity profiles and pseudo-colored threshold images were performed using the ImageJ software (US National Institute of Health). Statistical comparison of datasets was performed by two-tailed Student's *t* test.